Development and application of interferometric on-machine surface measurement for ultra-precision turning process

Duo Li

EPSRC Future Metrology Hub, University of Huddersfield

EPSRC Future Metrology Hub, Queensgate, Huddersfield, HD1 3DH, United Kingdom

e-mail: duo.li@hud.ac.uk

Xiangqian Jiang

EPSRC Future Metrology Hub, University of Huddersfield

EPSRC Future Metrology Hub, Queensgate, Huddersfield, HD1 3DH, United Kingdom

e-mail: x.jiang@hud.ac.uk

Zhen Tong

EPSRC Future Metrology Hub, University of Huddersfield

EPSRC Future Metrology Hub, Queensgate, Huddersfield, HD1 3DH, United Kingdom

e-mail: z.tong@hud.ac.uk

Liam Blunt

EPSRC Future Metrology Hub, University of Huddersfield

EPSRC Future Metrology Hub, Queensgate, Huddersfield, HD1 3DH, United Kingdom

e-mail: l.a.blunt@hud.ac.uk

Abstract

The continuing evolution of ultra-precision machining places an increasing need to perform surface measurement in the manufacturing environment. Development of on-machine surface measurement (OMSM) tools for ultra-precision machining processes will enable the reduction of measurement cycle time as well as the potential improvement of machining accuracy. In the present study, an in-house designed interferometer probe is integrated onto an ultra-precision diamond turning machine. System configuration, calibration scheme and various scanning strategies are firstly presented. The benefit of OMSM preserves the consistency between the machining and measurement coordinate system. Two applications of OMSM for ultra-precision turning process are further investigated. To further improve the surface accuracy, corrective machining is carried out based on the on-machine measured data. The profile accuracy of a cosine curve sample was improved after corrective machining with OMSM. Moreover, process investigation with OMSM was employed to model the effect of process parameters on the form error in ultra-precision cylindrical turning process. OMSM enables the consistent measurement of part coordinates for each experimental run which is critical for acquiring a deterministic response for empirical modelling. A reduced quadratic model was built by means of response surface methodology and verified by the test for significance of the regression model. The confirmation tests show that the model predicted value conformed to the experimental value with a difference less than 4%.

Keywords

Ultra-precision turning; On-machine surface measurement; Interferometry; Corrective machining; Process investigation;

1. Introduction

Ultra-precision turning is now capable of generating surfaces with sub-micrometre form accuracy and nanometre surface roughness, which are in high demand from the optical, electronic and aerospace industries [1, 2]. However, many factors such as environmental noise, machine structural errors, vibration and tool wear induces surface deviations from the design model [3-5]. Thus the process of surface metrology and compensation are indispensable in the further development of fundamental techniques for better surface accuracy [6]. Shifting the approach of metrology from offline, lab based solutions towards the use of metrology within manufacturing platforms is urgently demanded to further enhance measurement efficiency and smart manufacturing [7-9]. On-machine surface measurement (OMSM) can avoid the errors caused by repositioning workpieces, use the machine axes to extend the measuring range and improve the measuring efficiency [10, 11]. Particularly in ultra-precision machining process, the transportation of workpiece between machine tools and metrology platform is problematic.

In the past decades, investigations of on-machine metrology tools have been increasingly reported. Based on the working principle, OMSM can mainly be classified into contact [12, 13] and optical methods [14-18]. The selection of sensor types primarily depends on the application and requirement of the machining process. Suzuki *et al.* [19] integrated a tilted contact probing system to measure steep-angle aspheric optical parts on the grinding machine. The tilted angle configuration reduced the change in the probing friction force and thus increased the measurement

accuracy. Similarly, Chen *et al.* [20] employed an on-machine contact probe for the measurement of ultra-precision grinding of tungsten carbide aspheric moulds. The overall profile error after grinding was obtained by subtracting the target profile from the actual ground profile along the normal direction. Optimized grinding processes achieved profile accuracy of 177 nm (PV) with a roughness of 1.7 nm (Ra). Gao *et al.* [21] described an atomic force microscope (AFM) system to measure sinusoidal microstructures on a diamond turning machine. The metrology system with proposed alignment was able to accurately measure in a spiral path with nanometre resolution. Keferstein *et al.* [22] developed a chromatic confocal distance sensor for measurements onto a cylindrical grinding machine. The sensor based on the principle of chromatic aberration, was insensitive to surface reflectivity, and it could measure wide range of samples with differing reflectivity. This on-machine measurement tool provided quality assurance, reduction of setting-up and machining time. Danzl *et al.* [23] integrated an optical areal measurement sensor based on focus-variation technology with an EDM machining centre, to perform closed-loop machine-measurement processes. Up to a fourfold increase in machining accuracy, elimination of clamping errors, automated quality assurance, and shorter lead times at a better output ratio were achieved with the aid of on-machine measurement. Röttinger *et al.* [24] presented the setup of miniaturized deflectometry on a diamond turning machine and measured high-precision specular surfaces without re-chucking operation. The advantages of on-machine deflectometry include the environmental robustness and the capability of measuring arbitrary freeform with sub-micron accuracy without additional null testing. With the development of global calibration and parasitic reflections reduction, deflectometry is also heading towards the accuracy of interferometry. King [25] equipped a large Zeeko polishing machine with a Dynamic Fizeau interferometer (4D Fizcam

3000 unit) in order to develop an integrated solution for in-situ measurement of large concave optics up to 1 m in diameter. The single shot spatial phase shifting technique enabled the interferometer to be vibration insensitive adding to its feasibility for on-machine measurements. Additionally, a 4D white light interferometer for texture measurement and a laser tracker for radius measurement were mounted on the polishing machine.

From the literature review, it can be seen that optical measurement is faster and preferred over the contact method for ultra-precision machining process, as contact methods tend to scratch the soft and ultra-smooth surfaces. Most studies focused on the characteristics of measurement sensors on the machine. However, less attention has been paid to evaluate the holistic performance of OMSM and exploit the potential of machine-measurement closed loop processes for ultra-precision manufacturing.

In the paper, the OMSM system configuration and calibration scheme are introduced together with scanning path strategies. The consistency between the machining and measurement coordinate system is preserved. Two applications of OMSM for ultra-precision turning are then proposed in this work. Corrective machining with OMSM is carried out to further improve the surface form accuracy through modification of tool path according to the measured surface error. In addition, process investigation with OMSM is employed to model the effect of process parameters on surface form accuracy in ultra-precision cylindrical turning. Machining experiments for both OMSM applications are carried out to prove the effectiveness of OMSM to improve machining efficiency and accuracy.

2. Development and calibration of OMSM system

2.1 System configuration

An in-house designed interferometer probe, termed Dispersed Reference Interferometry (DRI) [26] is designed as a robust single point tool for the embedded surface measurement. DRI works on the principle of a modified Michelson interferometer with chromatic dispersion purposefully added in the reference arm, resulting in a wavelength dependent optical path length. The 0.6 nm resolution with 800 μm range makes it dynamic to measure precise complex geometries. The low coherence source lends the method to an optical fibre-based implementation, as the potential for remote configuration and miniaturization [27]. The DRI single probing system is integrated onto an ultra-precision turning machine (Nanoform 250 Ametek Precitech), equipped with two linear hydrostatic axes and a high precision air bearing spindle. The DRI probe is fixed beside the tool holder and along the Z axis direction as illustrated in Fig. 1. The measurement data from DRI OMSM is analyzed in DRI signal processing unit and then fed back to a personal computer for subsequent process control by modifying the motion command in the machine driving system. The DRI probe is aligned coaxially to the spindle rotational axis, by means of adjusting its perpendicularity to the machined flat and multiple scanning of a convex sphere sample. The fitted apex point can be considered as the coaxial position and is saved in the machine tool coordinate system. The selection of measurement paths primarily depends on the measurement tasks and surface feature distribution. In this system, multiple radial, multiple circular and spiral paths are employed for on-machine surface inspection (in Fig. 2). Among them, multiple radial paths are mainly applicable to measurement of radial surface features; multiple circular paths are applicable

to measurement of circumferential surface features; a spiral path is a continuous trajectory and an efficient way to measure the general freeform surfaces.

2.2 Calibration of OMSM system

As measuring conditions vary with machine configuration, probing system setup and measurement task, calibration of the OMSM system is a task specific process. The calibration scheme for this OMSM system includes on-machine vibration analysis, machine kinematic error mapping and compensation and linearity error correction. For example, DRI is a single point measurement tool and its performance is affected by the vibration on the machine. Under the optical lab test, the static noise level is 0.63nm RMS, which is considered as the resolution of the interferometric sensor [26]. When the DRI sensor was tested in the machine tool, the static measurement indicated 2.2nm RMS, which is nearly 4 times the DRI internal noise, indicating the machine tool environmental effect on the measurement. The increase of noise level results from the machine slides and the spindle as well as electromagnetic disturbance. Besides, the DRI probe is carried by the machine tool axes to perform surface measurement. Due to mechanical imperfections, wear of machine tool elements, and stage misalignments, the deviation from the programmed scanning path (known as kinematics error) will induce additional measurement errors. The above issues has been addressed in detail in the authors' previous work [28, 29].

To further evaluate the DRI OMSM measurement accuracy, a multiple step height sample was measured on-machine using multiple radial paths. The sample was designed with 4 step heights (1 μm, 2 μm, 4 μm, and 8 μm). The measurement result is shown in Fig. 3. Six radial profiles were measured at equal angles of 30°. Measurement range was from 10 mm to -10 mm and probing

speed was set at 2 mm/min. Fig. 4 illustrates the error plot for the multiple step height measurement. Measurement error was calculated as the deviation between multiple step height value of DRI measurement and that of calibrated white light interferometer (Talysurf CCI 3000, Taylor Hobson). The maximum error of step height measurement was evaluated as 14 nm. More OMSM experiment results has been presented in authors' previous work [28, 29], which indicate that the established OMSM has comparable measurement accuracy with commercial offline measurement in terms of form evaluation.

3. Applications of OMSM for ultra-precision turning

Integration of OMSM avoids the need to transport workpiece between measurement and machining environment and thus consistency between the two coordinate systems is preserved. Two potential applications, including corrective machining and process investigation with OMSM are explored to exploit the integration benefits to further enhance the ultra-precision turning performance.

3.1 Corrective machining with OMSM

The presence of certain amount of form error of machined parts results from the environmental factors, machine dynamic errors, tool setting error and tool wear [3]. The integration of OMSM fundamentally avoids the alignment error between the measurement and machine coordinate datum. A corrective machining based on the proposed OMSM was developed to further improve the machined surface accuracy in a deterministic manner.

The experimental setup of corrective machining with OMSM is shown in Fig. 5. The DRI fibre-linked probe is mounted on to a manual adjustment stage for the purpose of the alignment process and the DRI measurement setup is installed beside the diamond tool holder on the Z axis.

A framework of corrective machining with OMSM is proposed, as illustrated in Fig. 6. According to the surface design and specification, proper machining and OMSM parameters are firstly selected. Following the machining process, the sample surface can be directly measured on-machine without removing and remounting operations. Data from on-machine measurement, represented as point clouds, is then compared with the design model. The overall surface error is obtained by subtracting the design surface from the measurement along Z direction. If the characterised surface error is larger than the pre-defined threshold, a corrective machining cycle is necessitated. As the coordinate datum for machining and measurement is preserved with the aid of OMSM, the derived surface error map can be directly used to generate a compensation tool path for corrective machining. The new tool path for corrective machining process is generated by superposing the processed surface error on the original tool path.

In order to conduct the corrective machining, surface error have to be derived from OMSM results and subsequently processed to generate the correction tool path. Different scanning strategies are adopted according to measurement and correction tasks. OMSM data processing for profile correction is shown in Fig. 7. Multiple radial paths are adopted to extract the height data from rotationally symmetric surfaces. The processed profile is compared with the design model and the derived error is fed back to modify the original cutting path. In the conventional X-Z turning process, the cutting tool path is often programmed from the sample border to the rotational centre.

As the multiple radial scanning paths move across the sample diameter, averaging and symmetric folding of the profile data should be performed.

A 2D profile error correction experiment of a cosine curve sample ($Z = A\cos(2\pi/\lambda\ X)$ with A =5 μm and λ =2.5 mm) was carried out. The machining and diamond tool parameters (Contour Fine Tooling) are listed in Table 1. Profile corrective machining is performed under the conventional X-Z turning mode.

After machining, multiple radial path measurement was adopted for the OMSM of this rotationally symmetrical surface. Six measurement profiles were spaced across the surface at equal angles (30°), as shown in Fig. 8. The measurement span was 4 mm to -4 mm along the radial direction and the scanning speed was set to be 2 mm/min.

Subsequently, multiple radial measurement results were compared with CAD design model and symmetric folding of the profile error was carried out, which is illustrated in Fig. 9. A new tool path for profile correction was subsequently generated by superposing the processed error on the original tool path. Corrective machining and tool parameters were kept the same as shown in Table 1. Profile error before and after correction process was plotted and compared in Fig. 10. The experiment results show that the profile accuracy was improved from 104.7 nm (RMS) to 58.6 nm (RMS), which validated the effectiveness of proposed corrective methodology to improve profile accuracy with the result of OMSM. For further verification of OMSM measurement results, offline measurement was carried out on a calibrated commercial stylus profilometer (Form Talysurf Series 2 PGI, Taylor Hobson, UK). Results shown in Fig. 11 and characterization results in the Table 2 indicate that DRI OMSM result conforms to the offline measurement in terms of form evaluation.

3.2 Process investigation with OMSM

An experimental investigation of process parameters together with reliable metrology feedback is considered indispensable in order to achieve demanding form accuracy in ultra-precision turning. The consistency between machining and measurement coordinates can be preserved with the application of OMSM, which fundamentally avoids the measurement deviation caused by re-positioning the workpiece after each experimental run.

This section will propose an empirical quadratic model to predict the machined surface form error under different processing parameters (spindle speed S, feedrate f and depth of cut a_p) with the aid of OMSM. The flow chart of the proposed process investigation methodology is illustrated in Fig. 12. The objectives, factors, and constraints need to be set before the experimental investigation. One-factor-at-a-time experimental approach is often time-consuming and has been gradually replaced by design of experiment (DOE) [30]. In this work, experimental response surface methodology (RSM) [30] is adopted to develop the statistical relationship between processing parameters and generated surface form accuracy. After the machine-measurement closed loop experimental run, the experiment data can be analyzed statistically by means of regression based on least squares method. OMSM plays a key role in the process investigation, as it is able to enhance automation, reduce transfer risk and allow machined surfaces to be inspected in a more deterministic way without misalignment error.

A full quadratic model is employed in this study and the relationship between the response and input variables can be described as follows:

$$Y = \alpha_0 + \sum_{i=1}^{k} \alpha_i X_i + \sum_{i=1}^{k} \alpha_{ii} X_i^{\,2} + \sum_{i} \sum_{j} \alpha_{ij} X_i X_j + \varepsilon \quad (1)$$

where Y is the estimated response, X_i is the input variables and ε is the random error. α_i, α_{ii}, and α_{ij}, respectively represent the coefficients of the linear, quadratic and interaction terms. The model coefficients $\{\alpha\}$ need to be estimated using a regression method and determined from the following equation:

$$\alpha = \left[\alpha_0, \alpha_1, \cdots, \alpha_n\right]^T = (X^T X)^{-1} X^T \hat{Y} \quad (2)$$

where X^T is the transposed matrix of input variables X and $(X^T X)^{-1}$ is the inverse of the matrix $(X^T X)$. Furthermore, the analysis of variance (ANOVA) was applied to identify the significant influential factors from all tested parameters, and to validate the goodness of fit of each model coefficient for the established response surface model. Finally, confirmation experiments are carried out to determine the model validity and accuracy.

In this study, a trigonometric function curve, mathematically described as $Z = \mathrm{A}\sin(2\pi/\lambda\ X)$ with A = 2 um and λ = 1 mm, was fabricated on a brass cylinder with different process parameters followed by DRI OMSM. The OMSM setup for process investigation is shown in Fig. 13. Different from the system configuration shown in Fig. 5, the DRI probe is placed perpendicular to the cylindrical surface. The measurement length was set as 3.5 mm along the axial direction and speed scanning speed was set at 2 mm/min. When the probe scans along the Z direction, the axial profile of cylindrical workpiece can be acquired on-machine.

The experimental result are summarized in Table 3 and analyzed using Minitab 17 [31]. The statistical significance of the response surface model was evaluated using *P*-values. If *P*-values are less than 0.05 (95% confidence), the obtained models are considered to be statistically significant, which means the selected variable in the model have a significant effect on the response. A preliminary analysis was tested for a full quadratic response model. By means of removing the

insignificant terms, the resulting ANOVA for the reduced quadratic model is summarized in Table 6. The interaction terms between *f*, *S* and a_p are not of statistical significance and were eliminated from the model, thus not shown in the Table 6.

The analysis result indicates that all the terms in the reduced model are statistically significant. All linear and corresponding square terms are thus employed in the response surface model. Among them, spindle speed (*S*) is the most significant factor associated with the surface form error, contributing 51.34% to the total variation. This can be explained by the fact that spindle motion characteristics have a strong relationship with the rotational speed, resulting in the deviation of cutting trajectories in the cylindrical turning processes. This phenomenon is also observed in other researcher's work on ultra-precision turning processes [32, 33]. The lack of fit is insignificant as the *P*-value is 0.308, larger than 0.05 (level of significance), implying that the null hypothesis cannot be rejected. Besides, the determination coefficient R^2, defined as the proportion of the explained variation to the total variation, is 96.52% (close to 1), indicating the measured response data is well fitted. In addition, the plot of the fitted residuals in the observation is drawn in Fig. 14. A good agreement between the predicted and on-machine measured response value is observed.

With estimated regression coefficients for individual variable listed in Table 5, the reduced quadratic response surface model can be expressed as a mathematical function of machining parameters. This empirical equation can be also employed to predict the machined surface form error as follows:

$$Y = 45.43 + 14.49\, f - 0.1123\, S - 2.66\, a_p - 1.665\, f^2 + 0.000074\, S^2 + 0.2934\, a_p^{\,2} \qquad (3)$$

In order to visualize the interaction effect among the machining parameters, the 3D response graphs for the surface form error RMS values are plotted in Fig. 15(a), Fig. 15 (b) and Fig. 15 (c).

In each plot, there are two independent variables and the third factor is held constant at the middle level. The graphs illustrate that the form error of machined surface decreases with the lower level of feedrate and represents a concave form with depth of cut and spindle speed.

In order to validate the established model and evaluate the prediction accuracy, three confirmation tests were further performed. The experiment condition and measurement results are shown in Table 6. The model predicted values and the experimental values were compared and the difference lies within -3.81% to 2.31%. The results indicate that the developed response surface model based on OMSM data can be used to model and predict the cylindrical surface error within 95% confidence intervals ranges of parameters studied.

4. Conclusions

The paper presents the development and application of DRI OMSM system for ultra-precision turning process. System configuration, calibration scheme together with scanning path strategies was developed to validate the fidelity of OMSM results. The OMSM experiment of a multiple step height sample indicated the maximum measurement error was evaluated as 14 nm. Furthermore, consistency between the machining and measurement coordinate system is preserved with the OMSM integration.

Two applications of OMSM for ultra-precision turning were also investigated in this work. Corrective machining with OMSM was proposed to improve the profile/surface accuracy through modification of tool path according to the on-machine measured profile/surface error data. The experiment results show that the profile accuracy of a cosine curve sample was improved from 104.7 nm (RMS) to 58.6 nm (RMS) after corrective machining, which has validated the

effectiveness of the proposed corrective machining methodology with OMSM. Another application, process investigation with OMSM was employed to model the effect of process parameters on the form error in ultra-precision cylindrical turning process. The reduced quadratic model obtained by means of response surface methodology was verified by the test for significance of the regression model and goodness of fit. The spindle speed was the most significant factor influencing machined surface form error, with 51.34% contribution to the total variability. The confirmation tests showed the model predicted value conformed to the experimental value, with a difference less than 4%. In summary, the application of OMSM tools will contribute to the improvement of machining accuracy and process investigation performance for the ultra-precision turning process.

Acknowledgment

The authors appreciate Dr. James Williamson and Dr. Karl Walton for academic discussion of the current paper. The authors also would like to sincerely thank the reviewers for their valuable comments on this work.

Funding

This work is supported by the UK's Engineering and Physical Sciences Research Council (EPSRC) funding (Grant Ref: EP/P006930/1), the European Union's Horizon 2020 research and innovation Programme under grant agreement No 767589 and China Scholarship Council (CSC).

Nomenclature

$\{\alpha_i, \alpha_{ii}, \alpha_{ij}\}$ the coefficients of the linear, quadratic and interaction terms in response surface model

Adj MS	adjusted mean squares
Adj SS	adjusted sums of squares
ANOVA	analysis of variance
a_p	depth of cut
CAD	computer-aided design
DF	degrees of freedom
DOE	design of experiment
DRI	dispersed reference interferometer
f	feedrate
OMSM	on-machine surface measurement
PV	peak-to-valley
RMS	root-mean-square
RSM	response surface methodology
S	spindle speed
Seq SS	sequential sums of squares
X_i	input variables in response surface model
X^T	the transposed matrix of input variables X
$(X^TX)^{-1}$	the inverse of the matrix X^TX
Y	estimated response in response surface model
ε	random error in response surface model

References

[1] Brinksmeier, E., Gläbe, R., and Schönemann, L., 2012, "Review on diamond-machining processes for the generation of functional surface structures," CIRP Journal of Manufacturing Science and Technology, 5(1), pp. 1-7.

[2] Yu, D. P., Gan, S. W., San Wong, Y., Hong, G. S., Rahman, M., and Yao, J., 2012, "Optimized tool path generation for fast tool servo diamond turning of micro-structured surfaces," The International Journal of Advanced Manufacturing Technology, 63(9-12), pp. 1137-1152.

[3] Ramesh, R., Mannan, M., and Poo, A., 2000, "Error compensation in machine tools—a review: part I: geometric, cutting-force induced and fixture-dependent errors," International Journal of Machine Tools and Manufacture, 40(9), pp. 1235-1256.

[4] Schwenke, H., Knapp, W., Haitjema, H., Weckenmann, A., Schmitt, R., and Delbressine, F., 2008, "Geometric error measurement and compensation of machines—an update," CIRP Annals-Manufacturing Technology, 57(2), pp. 660-675.

[5] Li, L., Collins, S. A., and Allen, Y. Y., 2010, "Optical effects of surface finish by ultraprecision single point diamond machining," Journal of Manufacturing Science and Engineering, 132(2), p. 021002.

[6] Blunt, L., and Jiang, X., 2003, Advanced techniques for assessment surface topography: development of a basis for 3D surface texture standards" surfstand", Elsevier.

[7] Jiang, X., 2012, "Precision surface measurement," Philosophical Transactions of the Royal Society of London A: Mathematical, Physical and Engineering Sciences, 370(1973), pp. 4089-4114.

[8] Jiang, X., Wang, K., Gao, F., and Muhamedsalih, H., 2010, "Fast surface measurement using wavelength scanning interferometry with compensation of environmental noise," Applied optics, 49(15), pp. 2903-2909.

[9] Jiang, X., and Whitehouse, D., 2006, "Miniaturized optical measurement methods for surface nanometrology," CIRP Annals-Manufacturing Technology, 55(1), pp. 577-580.

[10] Fang, F. Z., Zhang, X. D., Weckenmann, A., Zhang, G. X., and Evans, C., 2013, "Manufacturing and measurement of freeform optics," CIRP Annals - Manufacturing Technology, 62(2), pp. 823-846.

[11] Ibaraki, S., Kimura, Y., Nagai, Y., and Nishikawa, S., 2015, "Formulation of influence of machine geometric errors on five-axis on-machine scanning measurement by using a laser displacement sensor," Journal of Manufacturing Science and Engineering, 137(2), p. 021013.

[12] Zhu, W.-L., Yang, S., Ju, B.-F., Jiang, J., and Sun, A., 2016, "Scanning tunneling microscopy-based on-machine measurement for diamond fly cutting of micro-structured surfaces," Precision Engineering, 43, pp. 308-314.

[13] Dong, Z., Cheng, H., Ye, X., and Tam, H.-Y., 2014, "Developing on-machine 3D profile measurement for deterministic fabrication of aspheric mirrors," Applied optics, 53(22), pp. 4997-5007.

[14] Quinsat, Y., and Tournier, C., 2012, "In situ non-contact measurements of surface roughness," Precision Engineering, 36(1), pp. 97-103.

[15] Zhu, Y., Na, J., Pan, W., and Zhi, Y., 2013, "Discussions on on-machine measurement of aspheric lens-mold surface," Optik-International Journal for Light and Electron Optics, 124(20), pp. 4406-4411.

[16] Böhm, J., Vernes, A., Vorlaufer, G., and Vellekoop, M., 2010, "Online monitoring of a belt grinding process by using a light scattering method," Applied optics, 49(30), pp. 5891-5898.

[17] Gao, W., Tano, M., Sato, S., and Kiyono, S., 2006, "On-machine measurement of a cylindrical surface with sinusoidal micro-structures by an optical slope sensor," Precision Engineering, 30(3), pp. 274-279.
[18] Sawano, H., Takahashi, M., Yoshioka, H., Shinno, H., and Mitsui, K., 2011, "On-Machine Optical Surface Profile Measuring System for Nano-Machining," Int. J. of Automation Technology, 5(3), pp. 369-376.
[19] Suzuki, H., Onishi, T., Moriwaki, T., Fukuta, M., and Sugawara, J., 2008, "Development of a 45° tilted on-machine measuring system for small optical parts," CIRP Annals - Manufacturing Technology, 57(1), pp. 411-414.
[20] Chen, F. J., Yin, S. H., Huang, H., Ohmori, H., Wang, Y., Fan, Y. F., and Zhu, Y. J., 2010, "Profile error compensation in ultra-precision grinding of aspheric surfaces with on-machine measurement," International Journal of Machine Tools and Manufacture, 50(5), pp. 480-486.
[21] Gao, W., Aoki, J., Ju, B.-F., and Kiyono, S., 2007, "Surface profile measurement of a sinusoidal grid using an atomic force microscope on a diamond turning machine," Precision Engineering, 31(3), pp. 304-309.
[22] Keferstein, C. P., Honegger, D., Thurnherr, H., and Gschwend, B., 2008, "Process monitoring in non-circular grinding with optical sensor," CIRP Annals - Manufacturing Technology, 57(1), pp. 533-536.
[23] Danzl, R., Helmli, F., and Scherer, S., 2011, "Focus variation–A robust technology for high resolution optical 3D surface metrology," Strojniški vestnik-Journal of mechanical engineering, 57(3), pp. 245-256.
[24] Röttinger, C., Faber, C., Olesch, E., Häusler, G., Kurz, M., and Uhlmann, E., "Deflectometry for Ultra Precision Machining–Measuring without Rechucking," Proc. Proc. DGaO, p. P28.
[25] King, C. W., "Integrated On-Machine Metrology Systems," Proc. International Symposium on Ultraprecision Engineering and Nanotechnology (ISUPEN), Japan Society for Precision Engineering Semestrial Meeting 2010 JSPE Autumn Conference.
[26] Williamson, J., Martin, H., and Jiang, X., 2016, "High resolution position measurement from dispersed reference interferometry using template matching," Optics Express, 24(9), pp. 10103-10114.
[27] Williamson, J., 2016, "Dispersed reference interferometry for on-machine metrology," PhD thesis, University of Huddersfield.
[28] Li, D., Tong, Z., Jiang, X., Blunt, L., and Gao, F., 2018, "Calibration of an interferometric on-machine probing system on an ultra-precision turning machine," Measurement, 118, pp. 96-104.
[29] Li, D., Jiang, X., Tong, Z., and Blunt, L., 2018, "Kinematics Error Compensation for a Surface Measurement Probe on an Ultra-Precision Turning Machine," Micromachines, 9(7), p. 334.
[30] Montgomery, D. C., 2008, Design and analysis of experiments, John Wiley & Sons.
[31] Minitab, I., 2014, "MINITAB release 17: statistical software for windows," Minitab Inc, USA.
[32] Zhang, S., To, S., and Wang, H., 2013, "A theoretical and experimental investigation into five-DOF dynamic characteristics of an aerostatic bearing spindle in ultra-precision diamond turning," International Journal of Machine Tools and Manufacture, 71, pp. 1-10.
[33] Tauhiduzzaman, M., Yip, A., and Veldhuis, S., 2015, "Form error in diamond turning," Precision Engineering, 42, pp. 22-36.

1

1 **Figure Captions List**

2

3

1 **Table Caption List**

2

3

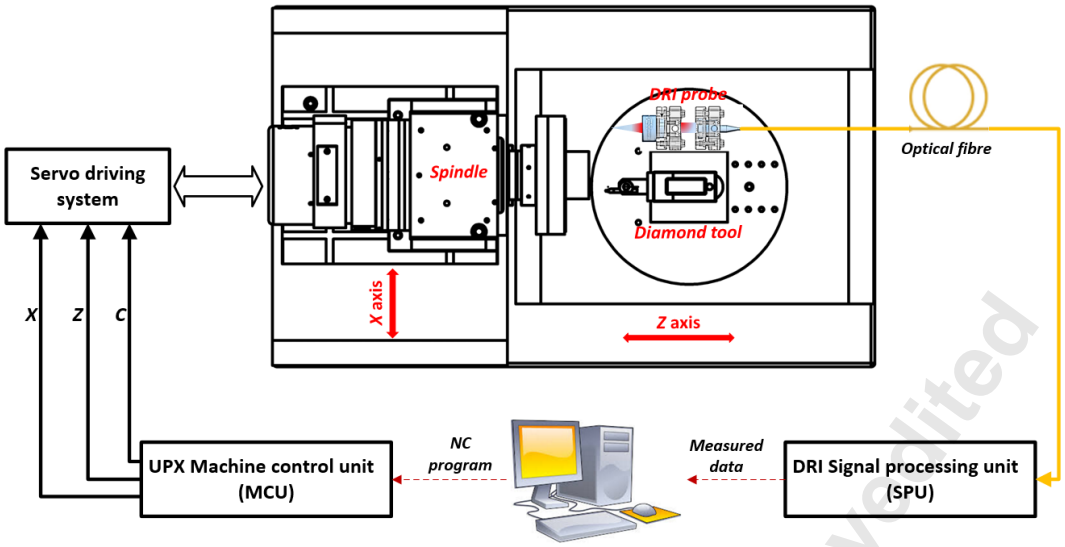

Fig. 1 OMSM system configuration on an ultra-precision turning machine

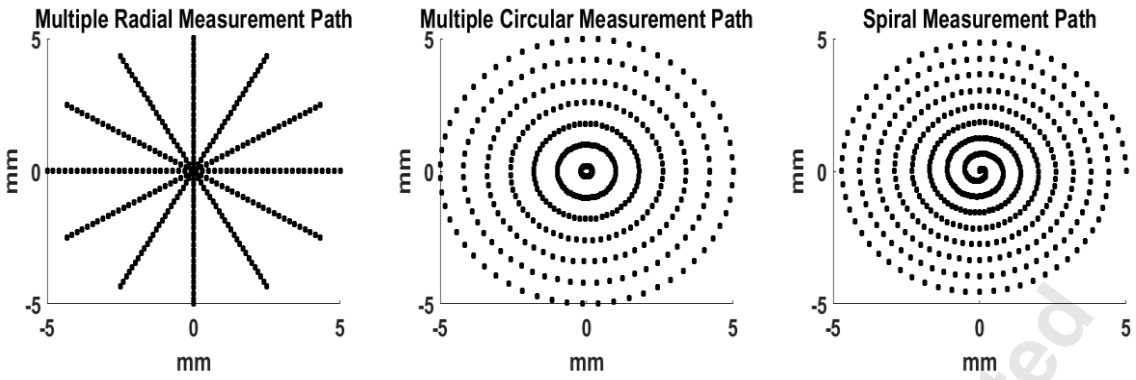

(a) **(b)** **(c)**

Fig. 2 Multiple radial (a), multiple circular (b), and spiral measurement path (c) for OMSM

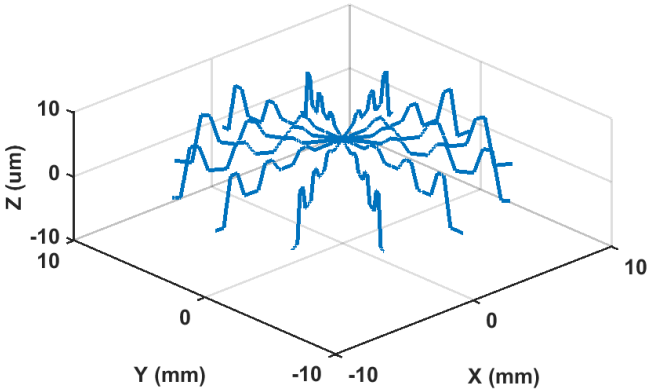

Fig. 3 OMSM of a multiple step height sample

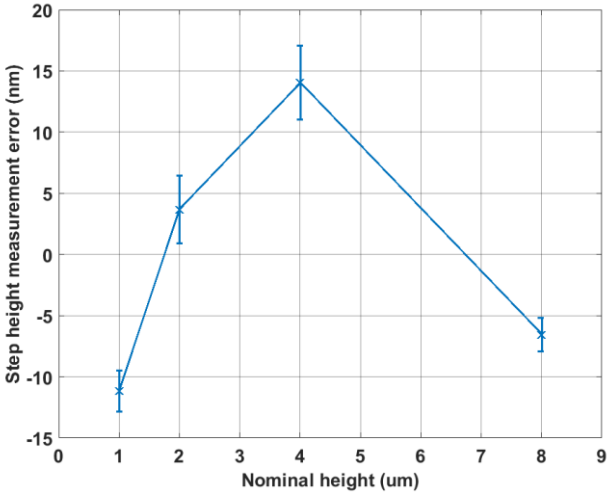

Fig. 4 Error plot of on-machine measurement of multiple step height sample

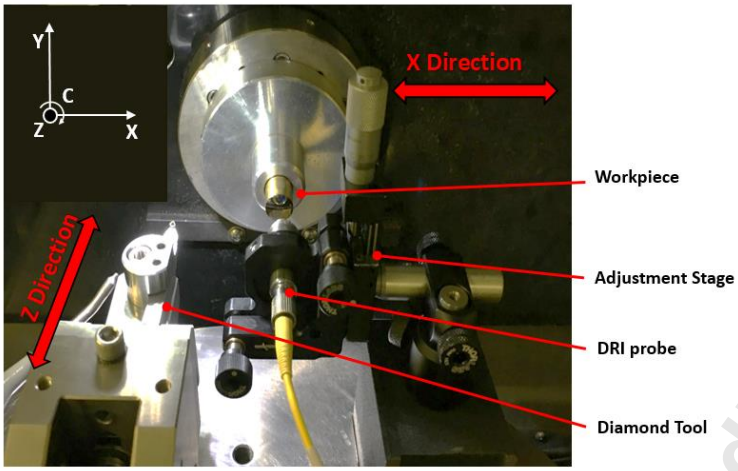

Fig. 5 OMSM setup for corrective machining

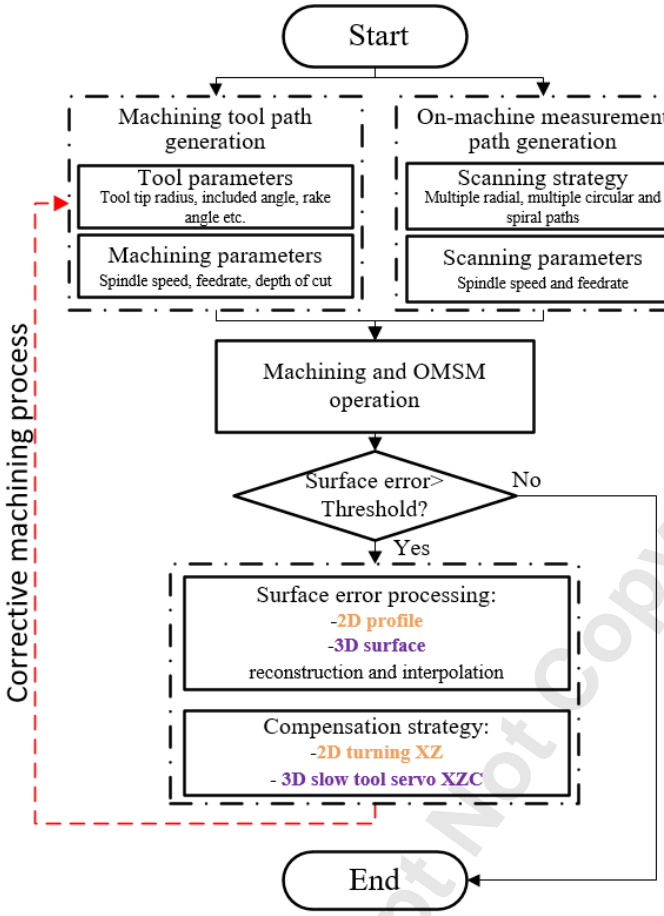

Fig. 6 Framework of corrective machining with OMSM

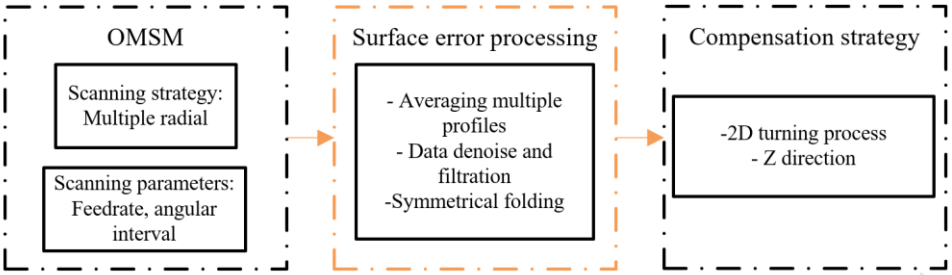

Fig. 7 OMSM data processing for profile corrective machining

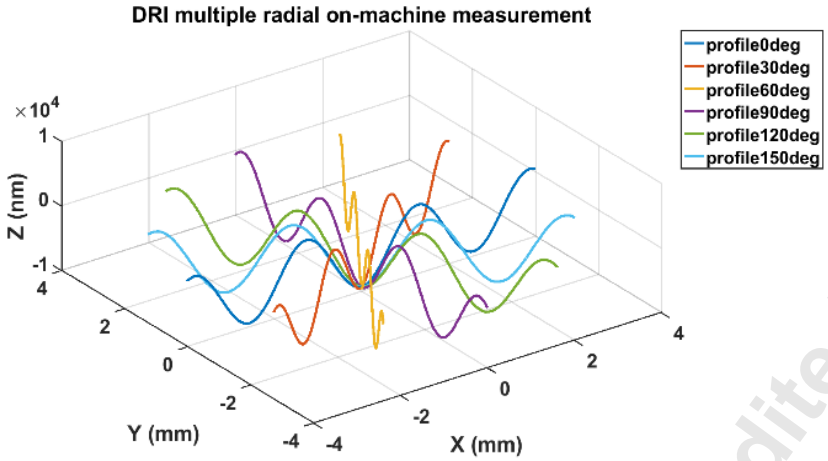

Fig. 8 OMSM of cosine curve sample

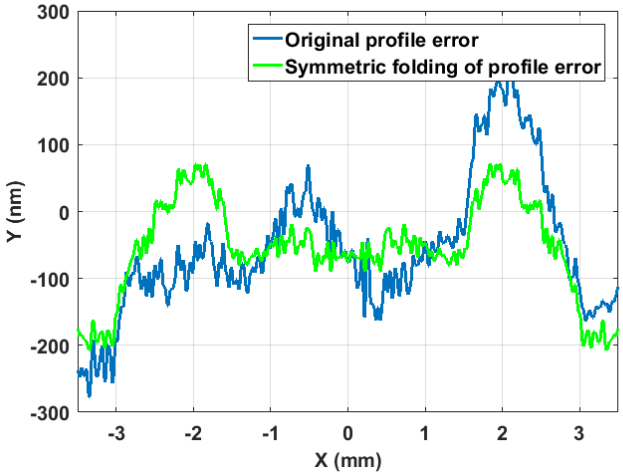

Fig. 9 Symmetric folding of profile error

1

2

3 **Fig. 10 Profile error correction results**

4

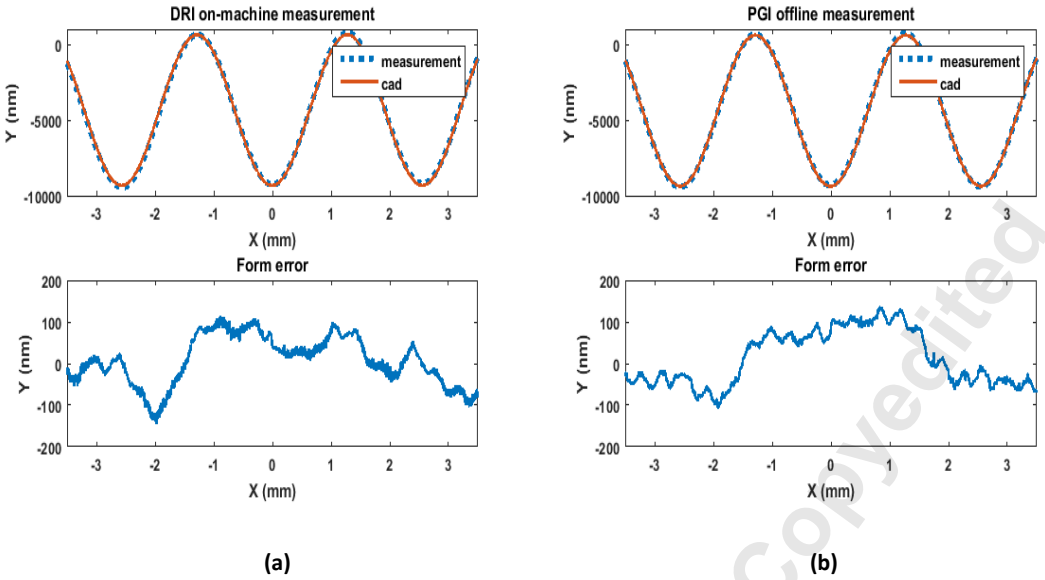

(a) (b)

Fig. 11 Measurement results and error analysis of DRI on-machine measurement (a) and PGI offline measurement (b) [28]

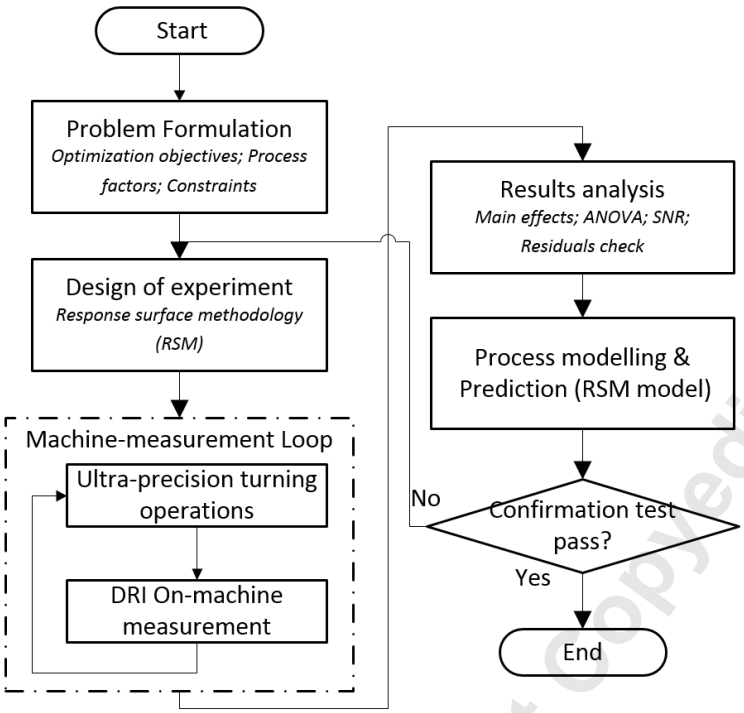

Fig. 12 Flow chart of process investigation strategy with OMSM

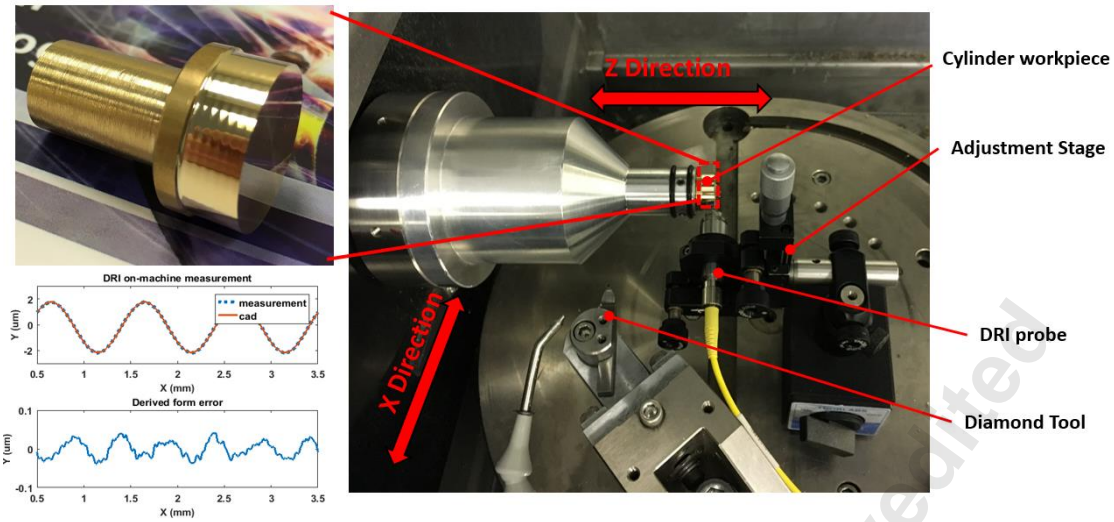

Fig. 13 OMSM setup for process investigation of cylindrical turning of cosine curve sample

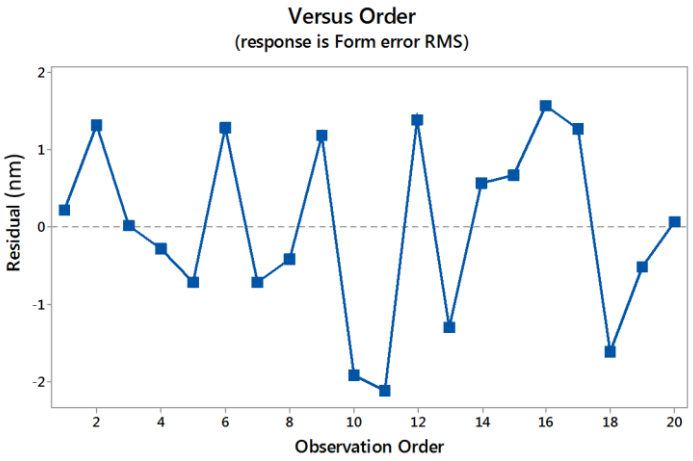

Fig. 14 Fitted residual plot in the observation order

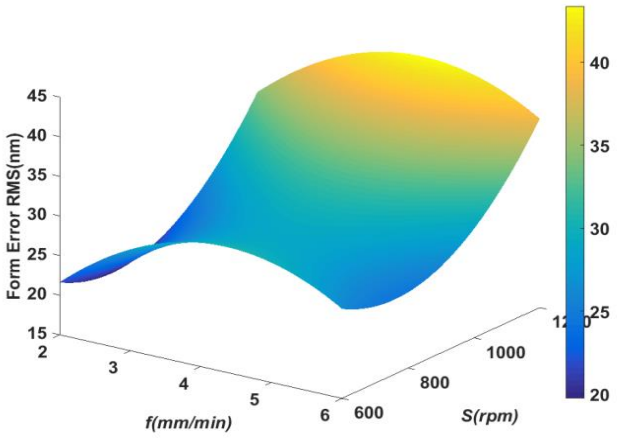

(a) Feedrate and spindle speed vs. form error RMS value

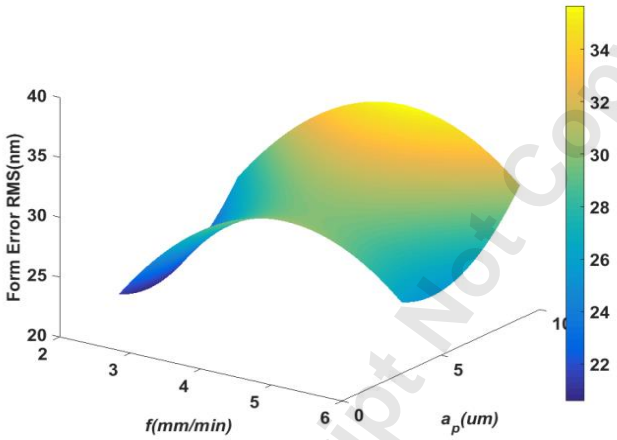

(b) Feedrate and depth of cut vs. form error RMS value

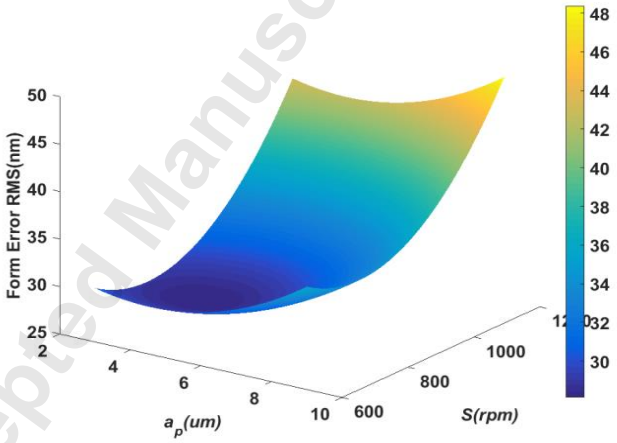

(c) Depth of cut and spindle speed vs. form error RMS value

Fig. 15 3D response surface graphs

Table 1 Machining and diamond tool parameters for cosine curve surface

Parameters	Value
Spindle Speed (rpm)	1000
Feedrate (mm/min)	0.5
Cutting depth (μm)	5
Tool radius (mm)	0.514
Included anlge (degree)	60

1 **Table 2 Characterization results of on-machine and offline measurement [28]**

Characterization parameter	DRI on-machine mean (standard deviation)	Offline mean (standard deviation)	Nominal deviation	Deviation (in %)
Fitted amplitude (µm)	4.974	4.982	0.008	1.6
Fitted frequency (mm^{-1})	0.390	0.391	0.001	2.6
Form error RMS (nm)	58.6	65.7	7.1	10.8

2

3

Table 3 Experimental design (CCD) and results of form error (OMSM)

Std run	Factors			Response
	Feedrate f (mm/min)	Spindle speed S (rpm)	Depth of cut a_p (μm)	Measured form error RMS (nm)
1	2	600	3	21.8
2	6	600	3	27.6
3	2	1200	3	33.9
4	6	1200	3	38.3
5	2	600	9	26.0
6	6	600	9	32.7
7	2	1200	9	38.3
8	6	1200	9	43.3
9	2	900	6	22.2
10	6	900	6	23.8
11	4	600	6	28.4
12	4	1200	6	44.2
13	4	900	3	28.8
14	4	900	9	35.8
15	4	900	6	30.7
16	4	900	6	31.6
17	4	900	6	31.3
18	4	900	6	28.4
19	4	900	6	29.5
20	4	900	6	30.1

1

2 **Table 4 ANOVA table of response surface model**

Source	DF	Seq SS	Adj SS	Adj MS	*F*-value	*P*-value
Model	6	710.974	710.974	118.496	60.01	<0.0001
Linear	3	499.499	499.499	166.500	84.32	<0.0001
f	1	55.225	55.225	55.225	27.97	<0.0001
S	1	378.225	378.225	378.225	191.53	<0.0001
a_p	1	66.049	66.049	66.049	33.45	<0.0001
Square	3	211.475	211.475	211.475	35.70	<0.0001
f^2	1	5.941	121.945	121.945	61.75	<0.0001
S^2	1	186.355	121.280	121.280	61.42	<0.0001
a_p^2	1	19.180	19.180	19.180	9.71	0.008
Error	13	25.671	25.671	1.975		
Lack of fit	8	18.538	18.538	2.317	1.62	0.308
Pure error	5	7.133	7.133	1.427		
Total	19	736.645				

3

4

1 **Table 5 Coded coefficients of regression model**

Model term	Coded regression coefficient	Contribution
Constant	30.024	
F	2.350	7.50%
S	6.150	51.34%
a_p	-2.66	8.97%
f^2	-6.659	0.81%
S^2	6.641	25.30%
a_p^2	2.641	2.60%

2

3

1 **Table 6 Confirmation tests for process investigation**

Confirmation run	Factors			Response		
	f (mm/min)	S (rpm)	a_p (μm)	Measured (nm)	Predicted (nm)	Error %
1	4	900	6	28.9	30.0	-3.81
2	6	600	6	26.7	26.2	1.87
3	2	1200	6	34.6	33.8	2.31

2

3

4